SLAC-PUB-10844
November 2004

Coverage effects on the magnetism of Fe/MgO(001) ultrathin films

C. Martínez Boubeta, C. Clavero, J.M. García-Martín, G. Armelles and A. Cebollada [(a)]

Instituto de Microelectrónica de Madrid-IMM (CNM-CSIC), Isaac Newton 8-PTM. 28760 Tres Cantos, Madrid, Spain.

Ll. Balcells

Instituto de Ciencia de Materiales de Barcelona-ICMAB (CSIC), Campus de la Universitat Autònoma de Barcelona. 08193 Bellaterra, Catalunya, Spain.

J. L. Menéndez.

Institut d'Electronique Fondamentale. Université Paris Sud, Bât. 220. 91405 Orsay CedeX. France

F. Peiró and A. Cornet

EME Electronic Materials and Engineering, Dept. Electronics, University of Barcelona, Martí i Franquès 1, 08028 Barcelona, Spain.

Michael F.Toney

Stanford Synchrotron Radiation Laboratory. 2575 Sand Hill Rd, M/S 69. Menlo Park, CA 94025, USA

Abstract

Different aspects of the structure-magnetism and morphology-magnetism correlation in the ultrathin limit are studied in epitaxial Fe films grown on MgO(001). In the initial stages of growth the presence of substrate steps, intrinsically higher than an Fe atomic layer, prevent connection between Fe islands and hence the formation of large volume magnetic regions. This is proposed as an explanation to the superparamagnetic nature of ultrathin Fe films grown on MgO in addition to the usually considered islanded, or Vollmer-Weber, growth. Using this model, we explain the observed transition from superparamagnetism to ferromagnetism for Fe coverages

Work supported in part by the Department of Energy Contract DE-AC02-76SF00515

Stanford Synchrotron Radiation Laboratory, Stanford Linear Accelerator Center, Stanford University, Stanford, CA 94309

above 3 monolayers (ML). However, even though ferromagnetism and magnetocrystalline anisotropy are observed for 4ML, complete coverage of the MgO substrate by the Fe ultrathin films only occurs around 6 ML as determined by polar Kerr spectra and simulations that consider different coverage situations. In annealed 3.5 ML Fe films, shape or configurational anisotropy dominates the intrinsic magnetocrystalline anisotropy, due to an annealing induced continuous to islanded morphological transition. A small interface anisotropy in thicker films is observed, probably due to dislocations observed at the Fe/MgO(001) interface

PACS. 61.10.Kw, 75.70.Ak, 78.20.Ls

(a) Electronic mail: alfonso@imm.cnm.csic.es

I. Introduction

The Fe/MgO(001) system is an excellent candidate to investigate the correlation between atomic structure and magnetism in low dimensional heterostructures. First grown almost 30 years ago [1, 2], this system's structural simplicity also makes it attractive from the theoretical point of view [3]. In bulk iron, the spin moment is weakened compared to an isolated Fe atom and the crystal field quenches the orbital moment. As predicted by Hund's rules, the reduced dimensionality should restore the free atom nature of Fe, and thus the net magnetic moment (M) would be enhanced. In this way, Li and Freeman [3] calculated a "giant" magnetic moment of 3.07 μB for a monolayer (ML) of Fe on a non-interacting MgO(001) substrate. However, from an experimental point of view, it is not straightforward to obtain a continuous, monolayer thick Fe film that fully covers the substrate to test these predictions, due to the formation of disconnected Fe islands several atoms thick in the first stages of growth [4, 5]. As a consequence, no giant magnetic moment has been experimentally found in this system so far [4, 6].

The reduction of the physical dimensions is likely to modify the electronic structure of the materials and therefore their magneto-optical activity. Such modification of the magneto-optical activity has been observed experimentally in Fe films due to the presence of quantum well states [7, 8, 9]. Furthermore, the magneto-optical properties of ultra thin magnetic layers may also be affected by the growth mode [10, 11], and hence, the assignment of changes in the magneto-optical spectra of ultra-thin films to changes in the electronic structure of the layers is not always clear.

With respect to magnetic anisotropies in the epitaxial Fe/MgO(001) system, a cubic anisotropy with the easy axis along the [100] and [010] directions is expected for thick films as this is found for bulk bcc Fe. In addition to this magnetocrystalline

anisotropy, different structural and morphological factors can be sources of additional contributions to the effective anisotropy experimentally obtained in epitaxial Fe/MgO(001) films. For example, Goryunov et al. [12] have reported an important surface anisotropy for film thicknesses around 1000 Å, which they attribute to strain relaxation extended as far as 45 Å from the film-substrate interface. Other reported sources of additional contributions to the magnetic anisotropy, usually of uniaxial character, are both deposition geometry, particularly for oblique-incidence of Fe on MgO(001) [13, 14, 15], and the presence of steps in the substrate [16]. It is also found that for 200 Å Fe films grown on MgO(001) the spatial morphology of the film (varying from continuous Fe films to dendritic like structures to islanded films) is a source of configurational anisotropy [17].

The goal of this study is to improve our understanding of the effect of lateral island connection and film continuity on the magnetic and magneto-optic properties of thin Fe films. Here we extend previous work, focusing on specific aspects of the structure-magnetism correlation in ultrathin Fe(001) films grown on MgO(001) substrates over a range of Fe thicknesses. An additional contribution of this work relies on the complementary in-situ and ex-situ characterization of the system with the use of MgO capping layers, which we show are more convenient than the standard metallic ones.

After a brief description of the deposition and experimental characterization techniques in section II, we describe in section III the methodology used to determine the thickness of ultrathin (down to a few atomic layers) Fe films by the use of X-ray reflectivity. Section IV will be devoted to study the onset of ferromagnetism in ultrathin Fe films and the role of the substrate terrace size in the transition from superparamagnetism to ferromagnetism. In section V we will exploit the high sensitivity

of the polar magneto-optical Kerr effect both on the partial vs full coverage and thickness of the Fe films to obtain a thorough picture of the magnetic and morphological nature of the grown structures. Finally, in section VI we describe how annealing induced structural modifications and interface effects influence the magnetic anisotropies of MgO/Fe/MgO(001).

II. Experimental

In this work, a multitechnique approach has been applied through the use of both in-situ and ex-situ characterization techniques. Sample preparation and in-situ characterization were carried out in a multichamber, ultra-high vacuum system equipped with sputtering and laser ablation facilities. Prior to Fe deposition onto MgO(001) commercial substrates (Mateck), a 100 Å MgO buffer layer was grown at 450 ºC by normal incidence pulsed laser deposition from a monocrystalline MgO target in the pressure regime of $7 \cdot 10^{-9}$ mbar. Fe layers were deposited at normal incidence onto this MgO buffer layer by triode sputtering at $4 \cdot 10^{-4}$ mbar Ar pressure. With these conditions, Fe grows with the well known Fe(001)[110] // MgO(001)[100] epitaxial relation [1, 2, 18], due to a good lattice match of MgO (a = 4.213 Å) and Fe (a = 2.866 Å) upon a 45º in-plane rotation, and additional sources for the magnetic anisotropy due to oblique deposition geometry are avoided. The Fe deposition rate was around 0.17 Å/s as calibrated by deposition time versus thickness measurements for Fe films several hundreds Ångstroms thick. The substrates were maintained at room temperature (RT) to avoid three dimensional (3D), island growth [19]. We define 1 ML as the atomic density of the bcc Fe (001) plane (= $1.22 \cdot 10^{15}$ atom/cm^2) and, in this study, Fe layers range in nominal thickness from 1 ML to 350 ML. Details on the growth mode and structure of this system in the thick film regime can be found elsewhere [19].

Reflection high-energy electron diffraction (RHEED) and transverse magneto-optical Kerr effect (MOKE) where used to characterize the films in-situ. For MOKE, hysteresis loops were measured using an He-Ne laser (wavelength 634.8nm) with a maximum magnetic field of 270 Oe. All the samples were capped with an epitaxial MgO layer, typically 100 Å thick and grown at RT, which did not modify the signal and coercive field of the hysteresis loop as measured in-situ before and after capping layer deposition. RT polar Kerr loops and polar Kerr spectra were obtained ex-situ with a maximum magnetic field of 16 kOe applied perpendicular to the sample plane. The polar Kerr spectra were measured for photon energies between 1.46 and 4.27 eV. Simulations of the Kerr spectra were obtained using a transfer matrix formalism [20]. The diagonal component (ε_{xx}) of the dielectric constant of Fe was taken from ref. [21] and the non diagonal component (ε_{xy}) obtained from the measured Polar Kerr rotation and ellipticity of a thick Fe film grown in the same conditions and capped with 70Å of MgO. Magnetization measurements were carried out by using a commercial Quantum Design SQUID magnetometer at RT and with a maximum magnetic field of 55 kOe applied parallel to the film plane. In all cases, the linear diamagnetic background from the MgO substrate and capping layers has been properly subtracted.

X-ray reflectivity experiments were performed in a four circle diffractometer with Cu Kα radiation and 0.25 degree divergence slits. The diffuse or background scattering was subtracted from the data to yield the specular reflectivity. It is important to note that X-ray reflectivity laterally averages over the instrumental coherence length, approximately one μm in our case. Hence, physical roughness will tend to smear the layers out, especially for thin layers (e.g., the Fe film). Simulations and fits were performed using the Parratt [22] formalism, which models the thin film structure as a series of layers. We used the following layers: the MgO buffer layer, Fe film and the

MgO cap layer, which was broken into an inner layer with a density near that of bulk MgO and a less dense layer due to reaction of the MgO with the ambient atmosphere. The roughness of the MgO-buffer layer/Fe and Fe/MgO-cap layer interfaces were fixed to be nearly equal, between 4-5 Å root-mean-square (rms). In all cases the roughness of the interfaces was assumed to be Gaussian.

III. Thickness determination of atomic layer thick Fe films

We have used X-ray reflectivity to determine the thickness of the ultrathin Fe films in our MgO/Fe/MgO structures. The power of this technique is twofold. First, it is based on its sensitivity to differences in electron density, and the use of substrate and cap layers with high contrast with respect to the ultrathin layer is an advantage. Second, this technique is especially sensitive in the case of symmetric structures, where deposition of a few atomic Fe layers means the generation of an artificial interface with the observation of the interference fringes due to the cap. To illustrate this, in Fig. 1 we show a comparison of reflectivity simulations for a set of Fe ultrathin films with different thickness grown on and capped with different materials. Cap layers are 50 Å thick (a common cap layer thickness) and a realistic 5 Å roughness in the air-cap, cap-Fe and Fe-substrate interfaces is included. In the non-symmetric Pt/Fe/MgO structure (Fig. 1(a)), it is nearly impossible to extract any information regarding the Fe layer, particularly for less than about 3 ML of Fe. Since substrate and cap are different materials, for 0 ML of Fe the oscillations due to the cap are already present, and deposition of a few atomic layers of Fe only slightly modify the reflectivity of the structure. The use of symmetric structures, however, (such as MgO/Fe/MgO, Pt/Fe/Pt and Al/Fe/Al as presented in Figs. 1(b)-(d)), gives rise to drastic changes in the reflectivity within the deposition of monolayered Fe films.

Having demonstrated the advantage of MgO cap layers, in Fig. 2(a) we show X-ray reflectivity results for the series of MgO/Fe/MgO fabricated samples. The best fits, which were used to extract the Fe thickness, are presented immediately below the experimental curves. The reflectivity curve for a "0" Å Fe sample, i.e. a structure where MgO buffer and capping layers were deposited under identical conditions as the rest of the series but with no Fe deposition, is also shown. As can be seen, deposition of just one atomic layer of Fe gives rise to the sudden appearance of interference fringes, absent in the sample without Fe. Even the before mentioned characteristic local minimum is well reproduced, the agreement between the experiment and model fit for the different samples being excellent and reproducing well positions and intensities of the different features. In Fig. 2 (b) we show as an example the electron density profile corresponding to the fit of the MgO/10 Å Fe/MgO sample. In the simulation the MgO buffer layer, deposited on the MgO substrate to planarize the surface, is also considered and its electronic density is found to be slightly larger than that of the substrate, although this layer does not have a big effect on the fit to the data. Since the thickness of the Fe layers is comparable to the rms interfacial roughness (about 4-5 Å), the Fe layer is smeared out and the thickness of the layer representing the Fe in the modeling does not accurately represent the Fe film thickness. Hence, we calculated an equivalent Fe thickness from the integrated areal density of the Fe layer (from the density profiles such as the Fig. 2 (b)) by dividing this by the bulk Fe electron density. With respect to the data modeling, this is a robust measure of the Fe film thickness. This formalism therefore allows a reasonable approach for the ex-situ determination of thickness of the atomic layer thick Fe films. The density corresponding to the MgO capping has two regions: an inner region with density similar to the MgO buffer, and an outer region

with much smaller electron density, probably due to the result of water adsorption from the air and/or brucite formation [23].

Figure 2(c) shows a compilation of Fe thickness from the reflectivity fits as a function of the nominal thickness. A linear behavior with a slope practically equal to 1 (0.94) is obtained, indicative of the 1 to 1 correspondence between nominal and actual deposited amount of material in the atomic layer limit; however, there is a non-zero offset thickness of 1.5 Å (approximately 1 Fe ML) nominal thickness. One possible explanation for this 1 Fe ML shift is a partial Fe oxidation at both interfaces [24, 25] with a total amount of oxidized Fe equivalent to 1 ML, giving rise to an Fe oxide that would have an electron density close to MgO, and therefore indistinguishable from the substrate and cap for X-ray reflectivity.

IV. The influence of substrate steps and film morphology on the onset of ferromagnetism in ultrathin Fe films

In all the films considered here the spontaneous magnetization at RT was in the film plane. Figure 3 shows transverse Kerr loops taken in-situ for uncapped Fe layers 2, 4, 6 and 210 ML thick. As is evident for the 2 ML film there is no ferromagnetic signal with the available magnetic field but there is instead a linear dependence of magnetization on applied field, which is probably due to the superparamagnetic nature of the film. No magnetic response was detected from the MgO substrate and capping layers in similar (RT) experiments. Also evident in Fig. 3 is the rapid onset of ferromagnetism with the addition of more Fe MLs (see also Fig. 8). For 4 ML, we observe the development of a magnetocrystalline anisotropy inherent to the bcc nature of Fe with easy and hard axes along [100] and [110] directions, respectively, and therefore equivalent to bulk Fe. These results are reasonably consistent with those

reported by Liu et al [4], who report ferromagnetic hysteresis at room temperature in uncapped Fe films measured in-situ for thickness above 4 ML.

It is remarkable that the loops obtained for the 4 to 210 ML Fe films (Fig. 3) are almost identical (except for the higher absolute Kerr signal for the thicker samples) with similar coercive fields; we believe that this is indicative of similar crystalline and morphological quality. Also apparent in Fig. 3 is the fourfold symmetry observed for the 4 ML sample, indicating either fully coverage of MgO by Fe or a large lateral size of the Fe covered regions, making magnetocrystalline anisotropy strong enough to dominate configurational or shape anisotropy and dipolar interactions present in non fully covered structures [17].

The absence of significant ferromagnetic response observed for Fe coverage below 3 ML may be due to three reasons: (a) the presence of a magnetic dead layer due to Fe oxidation at the top and bottom interfaces through reaction with MgO [24, 25], as evidenced by the X-ray reflectivity, (b) Vollmer Weber growth mode [26] that for such small coverage gives rise to superparamagnetic Fe islands and (c) a Curie temperature below RT (which is the measurement temperature), which in ultrathin films does not necessarily need to coincide with the bulk value, as observed for example in Co/Cu(001) [27].

To clarify this issue further, magnetic characterization was performed ex-situ using SQUID measurements at RT as shown in the inset to Fig. 4, once a linear diamagnetic background from the MgO substrate and capping layers has been subtracted. These magnetization curves indicate the presence of superparamagnetism for a Fe film of 2 ML and ferromagnetic behavior for thicker ones, 4 and 6 ML. From the SQUID measurements, in all the films, the Fe magnetic moment was that of bulk value within the error bar (see figure 4). However, considering the error bars in both the

determination of the films total magnetic moment and their Fe volume, more precise measurements are required to discard or prove the existence of a high magnetic moment at low thicknesses.

The superparamagnetism observed for 2 ML Fe, is consistent with the superparamagnetic relaxation of Fe deposited on MgO(001) previously reported by Adenwalla and co-workers [28, 29] and attributed to the presence of a distribution of Fe particles due to Volmer-Weber growth. Nevertheless, in our case, the rapid onset of ferromagnetism above 3 ML Fe indicates that the growth must not be too different from layer-by-layer, or that there are relatively flat islands that are laterally connected and form large magnetic regions, in contrast to Volmer-Weber growth, where more than about 3ML is required for the lateral connection between islands. The superparamagnetic nature found at low coverage in our case is more consistent with a picture of disconnected Fe platelets with volumes below the superparamagnetic limit. In addition to the Volmer-Weber growth reported by Liu et al. [4], there is an intrinsic mechanism that prevents the coalescence of Fe platelets when specifically grown on MgO and which is related with the step height in the substrate: the height of elementary steps in the MgO substrate is h = 2.1 Å along the (001) axis [30], while an Fe monolayer is 1.4 Å thick. Therefore, depositing only 1 ML Fe in a perfect layer-by-layer growth would result in isolated Fe platelets with lateral sizes equivalent to the MgO terrace size, but not connected to each other due to the height of the MgO steps. This lack of connection is an impediment for the formation of large Fe crystallites in the 1 ML regime, making it difficult to reach the volume to overcome the superparamagetnic limit at room temperature.

The superparamagnetic relaxation may be described by an Arrhenius law with a relaxation time given by

$$\tau = \tau_0 e^{KV/k_B T} \qquad (1)$$

where the precession time τ_0 is in the range of 10^{-12} s [31], K is the magnetic anisotropy per volume of individual particles with no interaction and V is the particle volume. Since the measurement time in our MOKE experiments is about 200 ms and the anisotropy constant for bulk iron is $K_1 = 4.6 \cdot 10^4$ J/m^3, the critical volume for superparamagnetism at room temperature becomes [32]

$$V_c = \frac{100\, k_B.T}{K_1} \approx 9\, x10^{-24}\ m^3 \qquad (2)$$

This in our case yields to a characteristic terrace area of $A_c = 6.29 \cdot 10^6$ Å^2 for monolayered (1.43 Å height) platelets, and therefore a characteristic length side (L_c) assuming squared terraces of 2500 Å. Superparamagnetic Fe platelets one atom thick should have lateral dimensions under this value. On the other hand, for thicknesses of 3 ML Fe ($A_c = 2.1 \cdot 10^6$ Å^2, $L_c = 1450$ Å) and above, the platelets would coalesce with those from adjacent terraces causing the film height to exceed the MgO step height and overcoming the volume threshold for superparamagnetism. The whole film would act as a ferromagnet. For a 2 ML Fe thickness, the height of the Fe layer is 2.87 Å, slightly above the 2.1 Å of the MgO step height, which together with the intrinsic roughness of both substrate and film, may produce a small overlap of the electronic clouds of Fe layers above and below a specific MgO step, with a weak exchange. But in the case of our 2 ML sample, we are far from this limit as illustrated by the superparamagnetic behavior in Fig. 4. By fitting the magnetization curve for the 2ML sample to the Langevin equation, we can estimate the effective number of spins per particle to be about 8000 Fe atoms. This leads to a corresponding lateral size for platelets close to 180

Å, well beneath the superparamagnetic limit as was discussed previously. Throughout this discussion, we have assumed that three-dimensional expressions (Eqs. (1) and (2)) can be applied to an ultrathin film. While we are unsure of the validity of this, we are aware of no models for superparamagnetism in monolayer thick films.

The critical length side of 1450 Å for a 3 ML Fe platelet compares well with the estimated terrace width (s) for a quasi ideal MgO(001) surface if we consider for example an $\alpha = 0.1^{\circ}$ miscut (typical in the substrates used in this work as checked by X-ray diffraction), which would yield MgO terraces with lateral dimensions $s = \frac{h}{tg\alpha} \approx 1200\text{Å}$ separated by monoatomic steps.

These results and their interpretation have important consequences: with the premise that 1 ML Fe layer with infinite lateral dimensions was ferromagnetic at zero temperature, the superparamagnetic or ferromagnetic nature of a real 1 ML Fe film grown on a MgO(001) substrate will depend on the lateral dimensions of the MgO terraces. Growth of a perfect continuous single ML Fe on MgO substrates with terraces larger than 2500 Å would give rise to a ferromagnetic Fe layer, while growth of an identical 1 ML Fe film on a substrate with terraces smaller than 2500 Å would give rise to a superparamagnetic layer. This implies that, in this specific case as in many others, experimental results from different groups or even from the same group in different periods of time are not directly comparable, since the onset of ferromagnetism in 1 ML Fe depends intrinsically on the substrate terrace size, which can vary from group to group and might even depend of the substrate preparation method.

Finally, in fig. 5 we present the ex-situ polar Kerr loops for the 2, 4, 6, and 8 ML samples. The Kerr signal for the superparamagnetic 2ML sample is very weak and that for the 4ML sample presents a linear behaviour with magnetic field, saturating at around 8 kOe. The saturation field then increases as we increase the amount of Fe, and for the 6

and 8 ML samples the saturation field is higher than the available magnetic field. Such reduction of the saturation field for the 4 ML can not be due to an out of plane magnetic anisotropy, as transverse Kerr loops shown in figure 3 indicate an in plane magnetization and, according to SQUID measurements, no reduction of Ms is observed. However the existence of steps in the MgO–film implies an intrinsic morphological roughness in the interface between MgO and Fe, which for the 4 ML films is of the order of the equivalent film thickness, therefore the out of plane demagnetizing factors could be strongly affected by such roughness [33] modifying also the saturation field.

V. Thickness and partial coverage dependence of the Kerr spectra in ultrathin Fe films

So far we have considered the influence of lateral island connection and growth mode on the onset of ferromagnetism in ultrathin Fe films, which can be established to be around 3 ML for our films. Nevertheless, the continuous character of the film may depend on the physical property analyzed. For example in figure 6 we present the experimental results of the Kerr rotation spectra for the 2, 4, 6 and 8 ML samples. As can be observed, the shapes of the spectra for the 6 and 8 ML samples are similar, with the magnitude of the Kerr rotation higher in the 8 ML case. However, the Kerr rotation spectra of the 2 and 4 ML samples are different from each other and different from the 6 and 8 ML. Moreover, in the same figure we present the simulations of the Kerr rotation spectra for the different samples assuming that they are continuous and fully cover the MgO substrate. As can be observed, the agreement between experiment and simulations is quite satisfactory for the 6 and 8 ML samples, while the agreement is much poorer for the 2 and 4 ML samples, suggesting that in these two samples the effective dielectric tensor of the layer is different from that of a continuous Fe film. According to the

preceding section, the magnetic properties of the 2 ML and 4 ML samples suggest that they are not completely continuous, and therefore the different behavior of the MO response for these layers may be due to the non continuous character of the films [10], but other effects, such as the modification of the electronic structure of the film [7], may also contribute to the modification of the MO response and can not be completely ruled out. Nevertheless, from a magneto-optical point of view, the transition to a continuous film occurs at about 6 ML. This character is maintained over a wide range of thicknesses. This is shown in figure 7, which presents the in-situ transverse Kerr magnetic induced change of the reflectivity, normalized to the reflectivity at zero field, as a function of the Fe thicknesses, together with a theoretical simulation assuming sharp Fe/MgO and vacuum/Fe interfaces. The agreement between the experimental points and the simulation curve is consistent with the complete coverage and therefore the continuous nature of the film for >5ML.

VI. Magnetic anisotropies: partial coverage, lateral connection and interface effects

In this section we will first consider the effect of annealing on the in plane structural configuration and therefore on the magnetic anisotropy of ultrathin films. As has already been mentioned, an indirect indication of the nearly continuous nature of the Fe films is the square hysteresis loops for thicknesses down to 4 ML. It has previously been observed in thicker Fe films [17] that an incomplete coverage resulting in dendritic structures or even Vollmer Weber growth produces the loss of the observed magnetic anisotropy, with rounded hysteresis loops independent of the direction of the applied magnetic field, due to the dominance of the configurational anisotropy over the

magnetocrystalline anisotropy. In ref. [34], it is reported that 10 ML Fe films with complete coverage on MgO(001) are unstable to annealing above 670 K and such annealing results in strongly islanded films. Bearing this in mind, we annealed our films and then examined the resulting change through MOKE measurements. The effect of annealing an uncapped 3.5 ML Fe film (grown at RT) at 400ºC for 10 minutes is illustrated in Fig. 8a and 8c, where hysteresis loops of the film before and after annealing are shown. Before annealing, the sample exhibits a square hysteresis loop when the magnetic field is applied along the easy direction, with a dominant magnetocrystalline anisotropy. However, after annealing the observed loop has a rounded shape, and it is independent of the orientation of the magnetic field relative to the crystallographic directions. This suggests the formation of interacting islands, with a broad reversal of the magnetization and higher coercivity due to the distribution of island sizes. The final island size and distribution will depend both on the initial Fe thickness and annealing temperature and duration. These observations are indicative of a transition from a nearly continuous to an islanded film, and corroborate the nearly continuous nature of the films before annealing. In contrast, for a somehow higher Fe coverage (14 ML in Fig. 8b and 8d) no change in the magnetization reversal is observed upon annealing at 400ºC. This suggests that the film is stable for this coverage, since, most likely, the Fe film covers completely the MgO surface and is too thick for there to be a massive displacement of material upon annealing or the kinetics for such restructuring are slow.

In order to shed light in the islanded structure of the annealed 3.5 ML films, which gives rise to equivalent hysteresis loops for field applied in the [100] and [110] directions, micromagnetic simulations have been performed with the OOMMF code [35]. The parameters are: exchange constant $A = 1.3 \cdot 10^{-6}$ erg/cm, saturation

magnetization M_s = 1700 emu/cm^3, cubic magnetocrystalline anisotropy with K = $4.6 \cdot 10^5$ erg/cm^3; the grid spacing is 2 nm, below the exchange length for iron. Two types of simulations have been performed: one assuming isolated particles with sizes large enough to be ferromagnetic at RT, and the other with clusters of particles (disk-like shaped) where the volume of the cluster is above the superparamagnetic limit at RT. In this latter case, the particles are assumed to be 1 nm thick, whereas their lateral size follows a Gaussian distribution with mean diameter of a few nanometers, which corresponds to the sizes observed by TEM in samples grown at high temperature [10]. When the particles are isolated, the simulated loops in the [100] and [110] directions are always different. On the other hand, if the particles are interconnected forming clusters there are some configurations where the loops in the [100] and [110] directions are equivalent, as shown in Fig. 8e for an ensemble of seventy-six interacting particles (mean diameter: 11 nm, standard deviation: 3 nm) randomly distributed over a 124×124 nm^2 area (see Fig. 8g). In this case three magnetic clusters are formed, shown in black, dark gray and light gray in Fig. 8g. In each cluster, there is a continuous path between any two spins, meaning that the particles interact not only by magnetostatics but also by exchange. On the other hand, particles belonging to different clusters can only interact via magnetostatics. Moreover, if all particles are connected so that the ensemble behaves now as one single cluster (see Fig. 8h), the loops obtained in the [100] and [110] directions are not equivalent, as shown in Fig. 8f. In particular, the remanence in the [100] direction is close to 1 and that in the [110] direction close to 0.7, which are the expected values for a continuous film with cubic anisotropy. The observed jumps in the hysteresis loops in the [100] direction are due to quasicoherent rotations of a large number of particles within the single cluster. This, in a real sample, is averaged out due to the much larger number of particles as compared to the simulation. Therefore, the

simulations strongly suggest that the annealing produces clusters of particles with no magnetic connection between the clusters. Finally, it is worth noticing that although the shape of the simulated loops in Fig. 8e is similar to that obtained experimentally, the coercivity is four times higher. Such discrepancy can be mainly attributed to the Brown's paradox [36]: in a real sample, not only thermal fluctuations but also any change in the anisotropy strength or direction (for instance around defects) can induce premature switching.

Besides this qualitative study, an estimate of the first-order anisotropy constants for the samples presented so far can be derived from the hysteresis loops along the [110] Fe hard axis. Applying the Stoner-Wohlfarth model [37] to describe this magnetization reversal as a coherent rotation, and taking into account a constant magnetic moment at all the coverages (1711 emu/cm^3 at room temperature (see Fig. 4)), this calculation yields an effective anisotropy constant K_{eff} of $5.96 \cdot 10^5$ erg/cm^3 for the 3 ML Fe film, while for the 350 ML film an anisotropy constant K_{eff} of $4.6 \cdot 10^5$ erg/cm^3 is obtained, identical to the value for K_1 of bulk Fe. To describe the magnetic anisotropy energy density constant as a function of the ferromagnetic thickness (*t*), we can assume both a volume (K_v) and interface contribution (K_s) to the anisotropy constant [38] as

$$K_{eff} = K_v + \frac{2.K_s}{t} \qquad (3).$$

In our case, and since the hysteresis loops remain unchanged by the MgO covering layer, according to Neél's theory on the fourfold in-plane anisotropy in bcc ferromagnets [39], we considered the sum K_s of both MgO/Fe and Fe/MgO interfaces. The experimental result gives $K_s \approx 1.7 \cdot 10^{-3} \pm 0.6 \cdot 10^{-3}$ erg/cm^2 for the Fe-MgO(001) interface (Fig. 9(a)). For comparison, this surface anisotropy term is an order of magnitude lower than the reported values for Fe on Au(001), Ag(001) and GaAs(001) [40, 41, 42, 43]. Because of the K_s positive value, we do not detect an in-plane spin

reorientation for decreasing thickness in (001)-oriented 2D Fe/MgO(001) films, as usually observed in Fe(001) films grown on Ag(001), Au(001), or GaAs(001) substrates [39].

There are several mechanisms that can give rise to thickness dependent magnetic properties in thin films, including the reduced symmetry at the surface or edges of atomic steps, intermixing of atoms at the interface, and strain. In this sense, the energy cost of homogeneous strain is proportional to the volume of the film, whereas the interface-dislocation energy to accommodate mismatch between the substrate lattice parameter and the deposited film would be proportional to its area. If we consider a pseudomorphic growth with a biaxial strain uniform throughout the film thickness, the magnetic pair-interaction energy between atoms is expressed in Legendre polynomials, and the (001) surface anisotropy energy for cubic structures is [44]

$$E_s = -\frac{8}{3} h\eta L(r_0)\cos^2\theta \qquad (4)$$

where h is the thickness of one monolayer, $L(r_0)$ is a Legendre polynomial with r_0 the bulk unstrained bond length, η the misfit and $\theta = 0,\pi$ for the magnetization vector **M** in the same plane as the misfitted interfaces [44]. Within this model we obtain a surface anisotropy $K_s \approx 1.6 \cdot 10^{-2}$ erg/cm^2 that is an order of magnitude larger than that calculated from figure 9, and therefore cannot account for the observed behavior.

On the other hand, it was suggested that magnetoelastic anisotropy falls as t^{-1} [38] if the strain in epitaxial films is relaxed via dislocations. We show in Fig. 9(b) a cross-sectional micrograph of the interface between the Fe film and the MgO substrate, observed along the [010] MgO zone axis. This TEM indicates the presence of misfit dislocations at the interface regularly distributed every 40 Å along [110] Fe planes, as shown by circles in the image. Similar conclusions are valid for the reciprocal MgO/Fe(001) interface (figures not shown). The elastic strain field ε resulting from the

introduction of an extra half plane for each edge dislocation (atoms are symmetrically arranged around the dislocation) is ε = 1.4/40 ≈ 0.036 and agrees well with the 3.8% misfit for the Fe-MgO system (assuming complete relaxation of the Fe layer). Therefore, the interface energy can be calculated from the change in the misfit energy resulting from the dislocations, with respect to the ideal strained crystal, as [38]

$$K_S \approx -B_1 t_c (\eta - \varepsilon) \qquad (5)$$

where $B_1 = -2.9 \cdot 10^7$ erg/cm^3 is the corresponding magnetoelastic coefficient for Fe. For Fe films in the ultrathin limit ($t_c \approx 10^{-8}$ cm), the resulting surface anisotropy is $K_S \approx 1 \cdot 10^{-3}$ erg/cm^2, closer to that observed experimentally. This suggests that the surface anisotropy in these films originates from misfit dislocations.

VII. Summary

Different aspects of the structure-magnetism correlation have been studied in epitaxial Fe films grown on MgO(001) in the atomic layer thickness range. An accurate thickness determination by standard X-ray reflectivity techniques is possible by the use of symmetric MgO/Fe/MgO structures. The observed transition from superparamagnetism to ferromagnetism is found at Fe coverages above 3 ML and is interpreted, in addition to possible Volmer-Weber growth, in terms of the substrate terrace size dependence of the Fe crystallites. The Fe ultrathin films become continuous and fully covering at around 6 ML, from both the morphological and magnetic point of view, as determined by polar Kerr spectra and simulations. Shape or configurational anisotropy dominates the intrinsic magnetocrystalline anisotropy in annealed Fe films under 6 ML, due to an annealing induced in plane reconstruction. A small interface anisotropy in thin films is observed, probably due to the relaxation of the Fe film at the Fe/MgO(001) interface.

Acknowledgements

The Spanish Commission of Science and Technology, and Comunidad de Madrid are acknowledged for financial support. Portions of this research were carried out at the Stanford Synchrotron Radiation Laboratory, a national user facility operated by Stanford University on behalf of the U.S. Department of Energy, Office of Basic Energy Sciences. One of the authors (J.M.G.M.) thanks the Spanish Ministry of Science and Technology for his present "Ramón y Cajal" contract.

Figure Captions

Figure 1. X-ray reflectivity simulations for a set of ultrathin Fe films of different thickness grown on and capped with different materials. Air-cap, cap-Fe and Fe-substrate interface roughness are 5 Å.

Figure 2. (a) X-ray reflectivity data and best fit for a series of MgO/Fe/ MgO samples with variable Fe thickness (best fit is shown below the corresponding experimental curve). The indicated Fe thicknesses are those extracted from fits. The reflectivity for a sample with MgO buffer and capping layers deposited under equivalent conditions but with no Fe deposition (labeled as 0 Å Fe) is also shown as a reference. (b) Electron density profile obtained from the fit of a representative sample. MgO electron density is $6.67 \cdot 10^{23}$ electrons/cm^3. (c) Fe thickness extracted from fits to XRR data versus nominal Fe thickness.

Figure 3. In-situ transverse Kerr hysteresis loops with the magnetic field applied along different directions (easy [100] Fe axis, hard [110] Fe axis) for 2 ML, 4 ML, 6 ML and 210 ML samples.

Figure 4. Calculated magnetic moment as a function of film thickness. Inset: in-plane hysteresis loops for the 2 ML, 4 ML and 6 ML samples from SQUID measurements at RT, once the background from the MgO substrate and capping layers has been subtracted. Dashed line for the 2ML curve is the fit to Langevin equation.

Figure 5. Polar Kerr hysteresis loops for the 2 ML, 4 ML, 6 ML and 8 ML samples.

Figures 6. Polar Kerr spectra for the same samples as figure 5; dots: experiment, lines: theoretical simulations assuming a Fe continuous layer 2ML, 4ML, 6ML and 8ML thick.

Figure 7. Fe thickness dependence of the transverse magneto-optical response for Fe/MgO(001) films. The continuous line is a simulation assuming a perfectly continuous film.

Figure 8. (a)-(d): In-situ transverse Kerr hysteresis loops for different Fe thin films. (a) 3.5 ML sample, as prepared. The field is applied along the [100] direction; (b) 14 ML sample, as prepared. The field is applied along the [100] direction; (c) 3.5 ML sample after annealing at 400º C. The two curves have been obtained with the field applied along the [100] and [110] directions; (d) 14 ML sample after annealing at 400º C. The field is applied along the [100] direction.

(e)-(f): simulated hysteresis loops for an ensemble of seventy-six iron particles. (e) the particles are interconnected forming three clusters; (f) the particles are interconnected forming a single cluster.

(g)-(h): particle distribution over a 124×124 nm^2 area for the simulations shown in (e) (with the three clusters shown in black, dark gray and light gray) and (f), respectively.

Figure 9. (a) Calculated effective anisotropy constant K_{eff} for different Fe thicknesses. The broken line is the fourfold bulk anisotropy constant K_1 for bulk Fe ($4.6 \cdot 10^5$ erg/cm^3), whereas the solid line is the fit to a 1/t dependence expected for an interface-type anisotropy. (b) HREM image (left) of a Fe/MgO(001) interface observed along the

[100] zone axis and corresponding Inverse Fast Fourier Transform image (right), filtered by the 020_{MgO} and 110_{Fe} spots, evidencing the appearance of misfit dislocations.

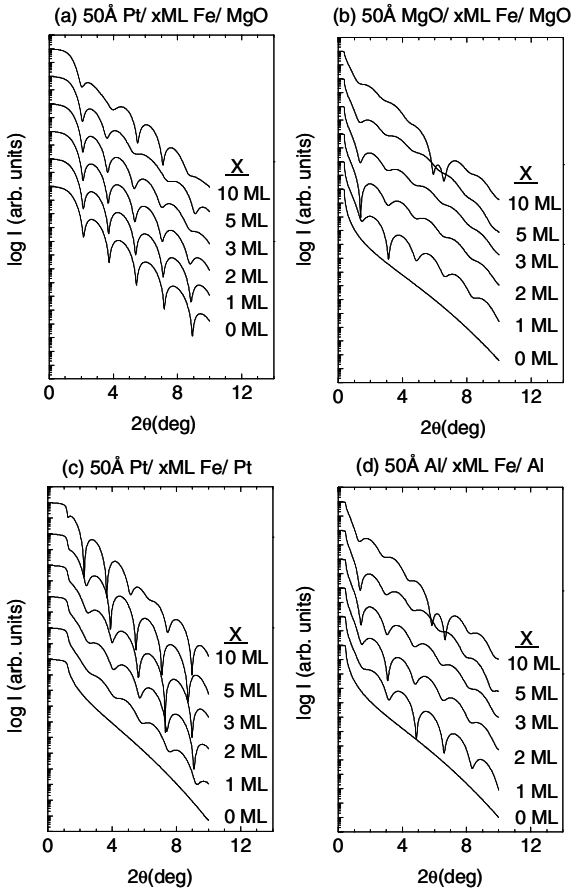

Fig. 1 – C. M. Boubeta et al., Phys. Rev. B

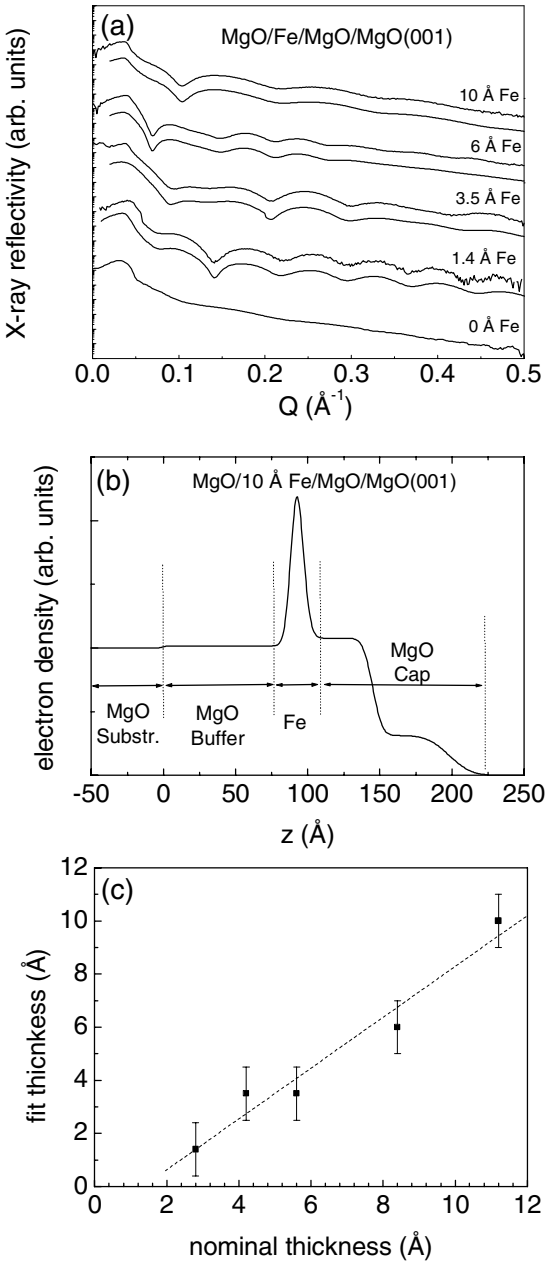

Fig. 2 – C. M. Boubeta et al., Phys. Rev. B

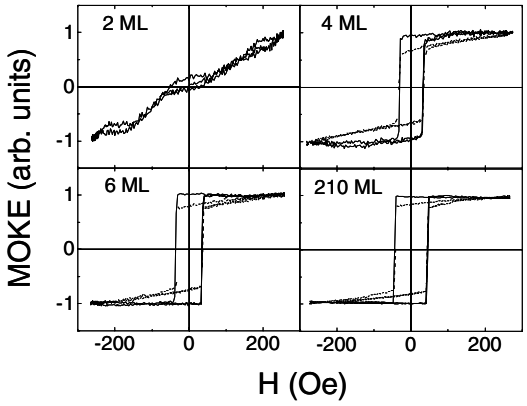

Fig. 3 – C. M. Boubeta et al., Phys. Rev. B

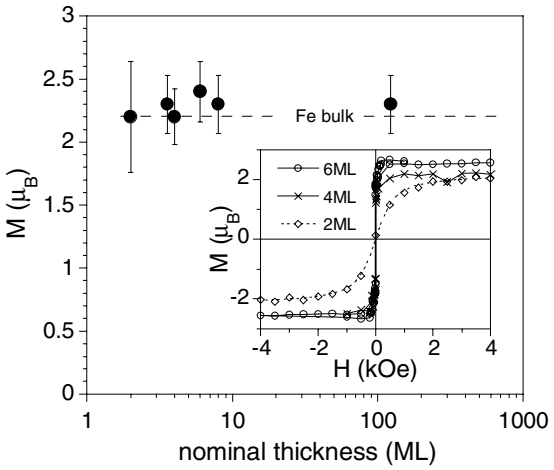

Fig. 4 – C. M. Boubeta et al., Phys. Rev. B

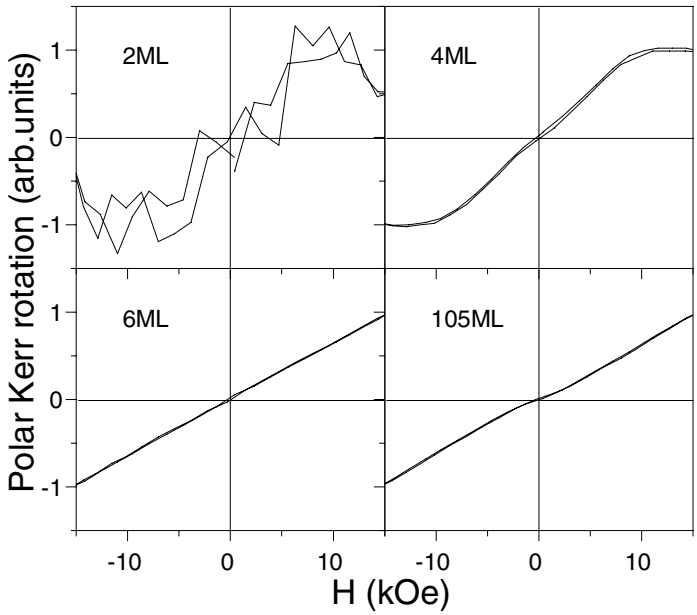

Fig. 5 – C. M. Boubeta et al., Phys. Rev. B

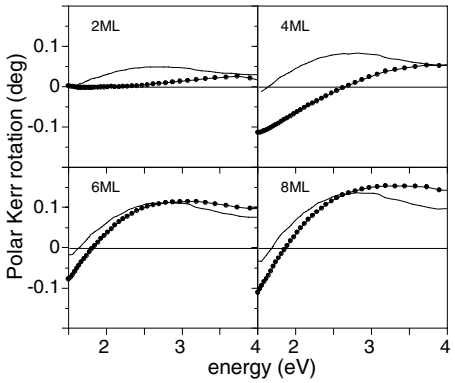

Fig. 6 – C. M. Boubeta et al., Phys. Rev. B

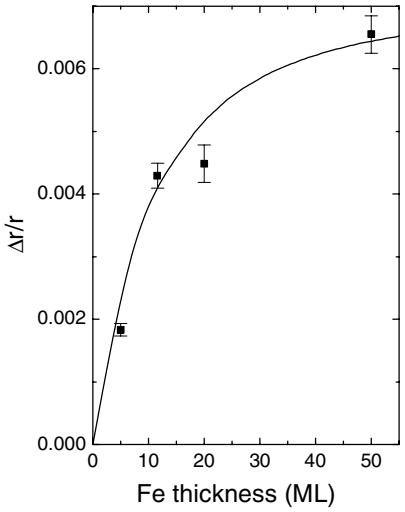

Fig. 7 – C. M. Boubeta et al., Phys. Rev. B

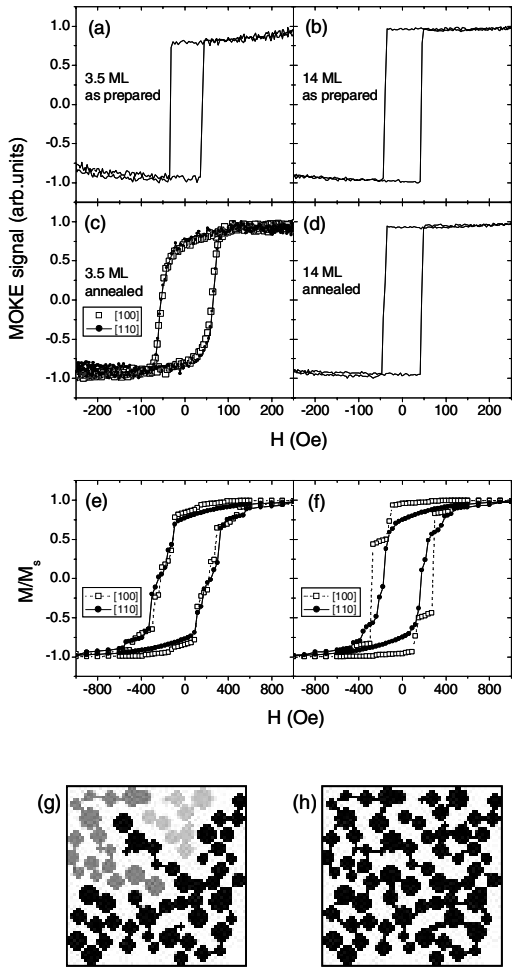

Fig. 8 – C. M. Boubeta et al., Phys. Rev. B

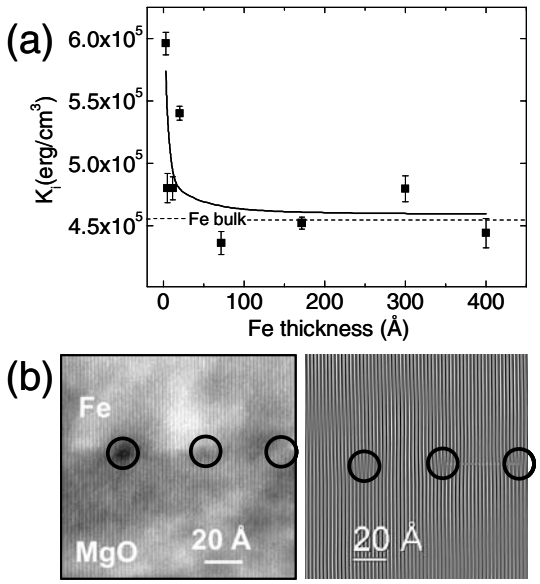

Fig. 9 – C. M. Boubeta et al., Phys. Rev. B

References

[1] T. Kanaji, K. Asano and S. Nagata, Vacuum **23**, 55 (1973).

[2] T. Kanaji, T. Kagotani and S. Nagata, Thin Solid Films **32**, 217 (1976).

[3] C. Li and A.J. Freeman, Phys. Rev. B **43**, 780 (1991).

[4] C. Liu, Y. Park and S. D. Bader, J. Magn. Magn. Mater. **111**, L225 (1992).

[5] B.M. Lairson, A.P. Payne, S. Brennan, N.M. Rensing, B.J. Daniels and B.M.J. Clemens, J. Appl. Phys. **78**, 4449 (1995).

[6] Y.Y. Huang, C. Liu and G.P. Felcher, Phys. Rev. B **47**, 183 (1993).

[7] Y. Suzuki, T. Katayama, S. Yoshida, K. Tanaka and K. Sato, Phys. Rev. Lett. **68**, 3355 (1992).

[8] W. Geerts, Y. Suzuki, T. Katayama, K. Tanaka, K. Ando and S. Yoshida, Phys. Rev. B **50**, 12581 (1994).

[9] R. Megy, A. Bounouh, Y. Suzuki, P. Beauvillain, P. Bruno, C. Chappert, B. Lecuyer and P. Veillet, Phys. Rev. B **51**, 5586 (1995).

[10] J.L. Menéndez, G. Armelles, A. Cebollada, C. Quintana, D. Ravelosona, C. Chappert, F. Peiró and A. Cornet, Appl. Phys. Lett. **81**, 1603 (2002).

[11] B. Sepulveda, Y. Huttel, C. Martinez Boubeta, A. Cebollada and G. Armelles, Phys. Rev. B **68**, 64401 (2003).

[12] Y.V. Goryunov, N.N. Garifyanov, G.G. Khaliullin, I.A. Garifullin, L.R. Tagirov, F. Schreiber, Th. Mühge and H. Zabel, Phys. Rev. B **52**, 13450 (1995).

[13] Y. Park, E.E. Fullerton and S.D. Bader, Appl. Phys. Lett. **66**, 2140 (1995).

[14] J.H. Wolfe, R.K. Kawakami, W.L. Ling, Z.Q. Qui, R. Arias and D.L. Mills, J. Magn. Magn. Mater. **232**, 36 (2001).

[15] O. Durand, J.R. Childress, P. Galtier, R. Bisaro and A. Schuhl, J. Magn. Magn. Mater. **145**, 111 (1995).

[16] J.L. Costa-Krämer, J.L. Menéndez, A. Cebollada, F. Briones, D. García and A. Hernando, J. Magn. Magn. Mater. **210/1-3**, 341 (2000).

[17] F. Cebollada, A. Hernando-Mañeru, A. Hernando, C. Martínez Boubeta, A. Cebollada and J.M. González Phys. Rev. B **66**, 174410 (2002).

[18] T. Urano and T. Kanaji, J. Phys. Soc. Japan **57**, 3043 (1988).

[19] C. Martínez Boubeta, E. Navarro, A. Cebollada, F. Briones, F. Peiró and A. Cornet, J. Cryst. Growth **226**, 223 (2001).

[20] M. Schubert, Phys. Rev. B **53**, 4265 (1996).

[21] J.H. Weaver, E. Colavita, D.W. Lynch and R. Rosei, Phys. Rev. B **19**, 3850 (1979).

[22] M.F. Toney and C. Thompson, J. Chem. Phys. **92**, 3781 (1990); V. Holy, U. Pietsch, T. Baumbach, in High-Resolution X-ray Scattering from Thin Films and Multilayers, Springer-Verlag, Berlin, 1998; M.F. Toney, C.M. Mate, K.A. Leach and D Pocker, J. Collid. Inter. Sci. **225**, 219 (2000).

[23] P. Liu, T. Kendelewicz, J.G.E. Brown and G.A. Parks, Surf. Sci. **412-413**, 287 (1998).

[24] H.L. Meyerheim, R. Popescu, J. Kirschner, N. Jedrecy, M. Sauvage-Simkin, B. Heinrich and R. Pinchaux, Phys. Rev. Lett. **87**, 076102 (2001).

[25] F.J. Palomares, C. Munuera, C. Martínez Boubeta and A. Cebollada. Applied Physics Letters (unpublished).

[26] M. Volmer and A. Weber, Z. Phys. Chem. **119**, 277 (1926).

[27] C.M. Schneider, P. Bressler, P. Schuster, J. Kirschner, J.J. de Miguel and R. Miranda, Phys. Rev. Lett. **64**, 1059 (1990).

[28] S. Adenwalla, Y. Park, G.P. Felcher and M. Teitelman, J. Appl. Phys. **76**, 6443 (1994).

[29] Y. Park, S. Adenwalla, G.P. Felcher and S.D. Bader, Phys. Rev. B **52**, 12779 (1995).

[30] K. Sangwal, P. Gorostiza, F. Sanz and J. Borc, Cryst. Res. Technol. **35**, 959 (2000).

[31] J.L. Dormann, D. Fiorani, and E. Tronc "Magnetic relaxation in fine-particles"; Advances in Chemical Physics, Volume XCVIII Pg. 283 (1997).

[32] A.H. Morrish, The Physical Principles of Magnetism. John Wiley & Sons, Inc. (1965).

[33] Y.P. Zhao, G. Palasantzas,G.C. Wang and J.T.M. DeHosson, Phys. Rev. B **60**, 1216 (1999).

[34] A. di Bona, C. Giovanardi and S. Valeri, Surf. Sci. **498**, 193 (2000).

[35] M. Donahue, D. Porter, R.D. McMichael, J. Eicke, URL http://math.nist.gov/oommf/.

[36] A. Aharoni, J. Appl. Phys. **90**, 4645 (2001).

[37] E.C. Stoner and E.P. Wohlfarth, Phil. Trans. R. Soc. A **240**, 599 (1948).

[38] P. Bruno and J.P. Renard, Appl. Phys. A **49**, 499 (1989).

[39] G. Bayreuther, M. Dumm, B. Uhl, R. Meier and W. Kipferl, J. Appl. Phys. **93**, 8230 (2003).

[40] M. Brockmann, M. Zölfl, S. Miethaner and G. Bayreuther, J. Magn. Magn. Mater. **198-199**, 384 (1999).

[41] B. Heinrich, Z. Celinski, J.F. Cochran, A.S. Arrott, and K. Myrtle. J. Appl. Phys. **70,** 5769 (1991).

[42] B. Heinrich, K.B. Urquhart, J.R. Dutcher, S.T. Purcell, J.F. Cochran, A.S. Arrott, D.A. Steigerwald, and W.F. Egelhoff, Jr., J. Appl. Phys. **63**, 3863 (1988).

[43] B. Heinrich and J.F. Cochran, Adv. Phys. **42**, 523 (1993).

[44] D.S. Chuang, C.A. Ballentine and R.C. O'Handley, Phys. Rev. B **49**, 15084 (1994).